Faraday Discussions

Cite this: *Faraday Discuss.*, 2018, **209**, 329

PAPER

2D graphene oxide channel for water transport

Baoxia Mi, * Sunxiang Zheng and Qingsong Tu

Received 12th February 2018, Accepted 5th April 2018
DOI: 10.1039/c8fd00026c

Layer-stacked graphene oxide (GO) membranes, in which unique two-dimensional (2D) water channels are formed between two neighboring GO nanosheets, have demonstrated great potential for aqueous phase separation. Subjects of crucial importance are to fundamentally understand the interlayer spacing (*i.e.* channel height) of GO membranes in an aqueous environment, elucidate the mechanisms for water transport within such 2D channels, and precisely control the interlayer spacing to tune the membrane separation capability for targeted applications. In this investigation, we used an integrated quartz crystal mass balance (QCM-D) and ellipsometry to experimentally monitor the interlayer spacing of GO, reduced GO and crosslinked GO in aqueous solution and found that crosslinking can effectively prevent GO from swelling and precisely control the interlayer spacing. We then used molecular dynamics simulations to study the mass transport inside the 2D channels and proved that the chemical functional groups on the GO plane dramatically slow down water transport in the channels. Our findings on GO structure and water transport provide a necessary basis for further tailoring and optimizing the design and fabrication of GO membranes in various separation applications.

Introduction

Graphene oxide (GO) nanosheets have been increasingly used as a two-dimensional (2D) material to create layer-stacked membranes for water purification and desalination.[1,2] The 2D nanochannels formed between two neighboring GO nanosheets serve as water transport channels and enable separation *via* either size exclusion (by precisely controlling the inter-layer spacing) or charge repulsion (by selectively manipulating the charged functional groups within channels).[3–7] Therefore, improving the performance of GO membranes depends largely on our understanding of the nanostructure, functionality and charge properties, and water transport mechanisms of the 2D channels in various aqueous solutions.

Department of Civil and Environmental Engineering, University of California, Berkeley, CA 94720, USA. E-mail: mib@berkeley.edu; Tel: +1 510 664 7446

As has been widely reported, when a restacked GO membrane is used for water separation, its interlayer spacing can be significantly enlarged due to water intercalation, thus decreasing membrane stability and separation capability.[8–10] By integrating the quartz crystal microbalance with dissipation (OCM-D) and ellipsometry, we have successfully characterized the swelling of un-crosslinked GO laminates in aqueous solution and found that the interlayer spacing can be enlarged from 0.8 nm in dry state to as high as 6–7 nm when fully hydrated.[9] The swelling is mainly attributed to the presence of hydrophilic, oxygenated functional groups on the edges and/or sticking out of the GO plane. Therefore, minimization of GO swelling requires GO to be, for example, partially reduced to remove the functional groups that cause swelling and/or chemically crosslinked by rigid, short bonds that enable precise spacing control. Despite numerous efforts to improve the stability and performance of GO membranes *via* reduction and crosslinking as two major strategies,[11–14] a complete understanding about the effectiveness of these strategies in controlling the GO swelling and interlayer spacing is still lacking.

Another significant knowledge gap in GO membranes is the true description of water transport behavior within the 2D channels. The very original motivation for creating layer-stacked GO membranes was a hope to achieve high water flux by taking advantage of the unimpeded water transport within graphene channels.[15] However, although the flux of GO membranes is typically higher than that of polymeric membranes,[8,16] the level of flux enhancement is far below 3–4 orders of magnitude as predicted by simulation work. A major reason for such a wide discrepancy is that it is still unclear how and to what degree the oxygenated functional groups on GO nanosheets would slow down water transport within the 2D channels.

In an effort to address the above knowledge gaps, we used an online monitoring system composed of QCM-D and ellipsometry to experimentally characterize the interlayer spacing of 2D channels in GO membranes that were prepared in pristine, reduced, and crosslinked states. The swelling behaviors of these membranes in an aqueous environment were critically compared. Meanwhile, we built computational models of GO and graphene to gain molecular-level insights into the influence of surface functionalization on water permeation in 2D channels and hence water transport behavior within a GO membrane.

Materials and methods

GO membrane synthesis

The GO suspension in water (0.02 mg mL^{-1}) was made by a modified Hummers' method as described in our previous work.[8] The pristine GO membrane was prepared by diluting 1 mL of the GO suspension 100 times and depositing the GO onto a commercial polyethersulfone (PES) membrane substrate (Sterlitech, Kent, WA) through vacuum filtration. In order to promote the alignment of GO nanosheets during vacuum filtration, a very low filtration speed ($\sim$1 mL min^{-1}) was used. The pristine GO membrane was then dried under vacuum and stored in a well purged desiccator for further treatment or testing.

To prepare the crosslinked GO (cGO) membrane, a pristine GO membrane was first pre-treated in humid air to stabilize the interlayer spacing. Specifically, a saturated $MgCl_2$ solution was prepared by dissolving an excessive amount of

$MgCl_2$ in DI water and sealed in a 1 L flask for 2 hours to generate a relative humidity of 34% in the head space. The humid air was then purged from the flask into a sealed reactor to allow the pristine GO membrane to gradually swell under exposure to the humid air and eventually gain a stabilized interlayer spacing. Then, 5 mL of ethylenediamine (EDA) liquid (Millipore/Sigma, Saint Louis, MO) was added to the reactor without direct contact with the GO membrane, and the reactor was heated to 80 °C to generate EDA vapor, which served as the crosslinker for the GO membrane. The GO membrane was exposed to EDA vapor for 1 hour to allow complete crosslinking reaction. Eventually, the EDA-crosslinked GO membrane was rinsed thoroughly with DI water to remove excessive EDA monomers.

To prepare the reduced cGO (rcGO) membrane, a cGO membrane was exposed to hydrazine vapor in a sealed reactor. The hydrazine vapor was generated by adding 1 mL of liquid hydrazine (Millipore/Sigma, Saint Louis, MO) into the reactor and heated to 60 °C. After exposure to hydrazine vapor for 1 hour at 60 °C, the cGO membrane was successfully reduced to rGO membrane, which was then rinsed thoroughly with DI water to remove excess hydrazine.

GO membrane characterization

The chemical compositions of the GO, cGO, and rcGO membranes were characterized by X-ray photoelectron spectroscopy (XPS) (PHI 5400, PerkinElmer). Atomic force microscopy (AFM) (Bruker Icon, Santa Barbara, CA) was used to illustrate the surface morphology and roughness of GO membranes in different stages of crosslinking and/or reduction. The interlayer spacing of each membrane in dry state was measured by X-ray diffraction (Bruker, Madison, WI).

To study the swelling behavior of the GO membrane before and after crosslinking, we used an integrated system consisting of QCM-D (E-1, Q-sense, Sweden) and ellipsometry (FS-1 Multi-wavelength, Film Sense, Lincoln, NE) to simultaneously measure the changes in mass and thickness, respectively, of the GO membrane in a humid environment (Fig. 1). To start the experiment, a pristine GO membrane formed on top of a PES support was transplanted onto a gold-coated quartz sensor following a detailed procedure described in our earlier publication.[9] The membrane-coated sensor was installed in the QCM-D chamber,

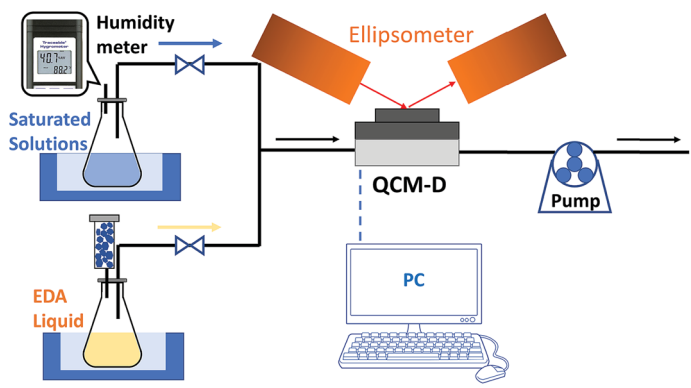

Fig. 1 Schematic illustration of the real-time monitoring of membrane interlayer spacing.

which has glass lenses on both sides to allow the optical characterization of membrane thickness by an ellipsometer. To mimic membrane synthesis procedures, air with a relative humidity of 34% and EDA vapor were driven into the QCM-D chamber by a peristaltic pump. Because of the limitation of the temperature setting in the QCM-D chamber and the need to prevent the condensation of liquid on the sensor (otherwise the film mass and thickness would be overestimated), the EDA liquid was heated to 40 °C while the temperature in the chamber was set to 60 °C. QCM-D and ellipsometry data were recorded in real-time during the crosslinking process. Afterwards, the sensor was taken out of the chamber, rinsed with DI water to remove residual EDA, dried in an oven, and installed back to measure the mass and thickness of the crosslinked GO thin film. The swelling behaviors of the pristine and crosslinked GO membranes were then monitored in air with relative humidities of 34%, 45% and 75%, which were generated by saturated solutions of $MgCl_2$, K_2CO_3, and NaCl, respectively. The QCM-D data (*i.e.* the oscillation frequency and energy dissipation) were analyzed to obtain the mass of the GO film, and the ellipsometry data were analyzed to determine the thickness of the GO film by fitting the dielectric constants using Cauchy's equation.

Membranes performance tests

The performances of the GO, cGO and rcGO membranes were each tested in a lab-scale reverse osmosis (RO) system as described in our previous study.[17] To test the membrane water flux, the membrane was first installed in the RO cell and compressed under 600 psi (41.4 bar) at 25 °C for 2 hours, and then the pure water flux was measured under 200 psi (13.8 bar) with DI water as feed. The weight of the permeate water was measured using a balance (Denver Instruments, Denver, CO) and automatically recorded by a computer. To test the separation performance, 100 mM $MgCl_2$ and Na_2SO_4 solutions were used as feed solution and the other operation conditions remained the same. To calculate the rejection rate, the ion concentrations of the feed and permeate water were measured by a conductivity meter (Accumet Excel XL30, Thermo Scientific, Marietta, OH).

Molecular dynamics simulation of the GO membrane and water transport

The molecular structure of GO primarily consists of hydroxyl and epoxy groups, which are randomly distributed on both sides of on the carbon plane, plus a smaller number of carboxyl groups, which decorate all of the carbon atoms on the edge of the sheet.[9] Based on our previous GO characterization,[9] the number ratios of hydroxyl and epoxy functional groups to carbon atoms are 10% and 9%, respectively. Considering the computational cost associated with molecular dynamics (MD) simulation, each GO sheet was built with lateral dimensions of 10 nm × 10 nm. Neighboring GO sheets on the same plane were spaced 2 nm apart to allow water molecules to enter the 2D channels almost freely. The interlayer spacing of the GO membrane was set to be 3 nm.

We carried out the MD simulation using GROMACS[18] and processed and visualized the simulation results using VMD.[19] The OPLS force fields[20] (eqn (1)) were used in the simulation.

$$V = \sum_{\text{bonds}} k_b(b - b_0)^2 + \sum_{\text{angles}} k_\theta(\theta - \theta_0)^2 + \sum_{\text{dih}} k_\phi[1 + \cos(n\phi - \delta)] + \sum_{\text{imp}} k_w(w - w_0)^2 + \sum_{\text{no bond}} \varepsilon\left[\left(\frac{\sigma}{r}\right)^{12} - \left(\frac{\sigma}{r}\right)^{6}\right] + \frac{q_i q_j}{\varepsilon_0 r_{ij}} \quad (1)$$

Each term accounts for the energy caused by different parts of the system, including bond stretch (V_{bond}), bond angle (V_{angle}), torsion angle (V_{dih}), out of plane bending (V_{imp}), van der Waals energy, and electrostatic energy. Potential parameters for sp^2 carbon atoms, functionalized carbon atoms, oxygen in functional groups, and bonding interactions including bond stretching, angle, and dihedral potentials in the GO model were all taken from previous literature.[21,22]

In order to eliminate surface effects and ensure a continuous flow of water molecules through the GO channel, periodic boundary conditions were imposed in all three dimensions. The water molecules were treated as a rigid body model,[23,24] which allowed the use of larger time steps in computation (2 fs in this study). Each system was simulated for 5 ns, followed by an equilibration under the Nose–Hoover thermostat[25] NVT ensemble (*i.e.* a constant number of atoms, fixed volume, and a constant temperature of 298 K). Then, the non-equilibrium MD simulation was performed[26] by adding constant acceleration in one direction for each atom. The PME (Particle-mesh Ewald) method was employed to account accurately for the long-range electrostatic interactions of the charges or ions and their periodic images.[27] The cut-off of the Lennard–Jones (LJ) interactions was set at 1.2 nm in all three directions. The neighbor list was updated at every step to avoid intrinsic errors.[28]

Results and discussion

Properties of dry pristine GO, cGO, and rcGO membranes

As shown in Fig. 2, the dry pristine GO membrane had a light brownish color and a surface roughness (R_q) of 5.6 nm. After crosslinking by EDA vapor, the dry membrane became darker and shinier with a slightly lowered surface roughness of 3.9 nm. The subsequent reduction by hydrazine further darkened the dry membrane and decreased the surface roughness to 2.3 nm. Note that the color change also depends on the thickness of the GO membrane, and the color is in general lighter with thinner membranes. The effectiveness of EDA crosslinking is confirmed by the XPS characterization (Fig. 3A), which exhibits a new N peak and slightly lowered O peak. At the same time, as shown in Fig. 3B, the interlayer spacing of a dry membrane was changed from a single peak at 0.79 nm for pristine GO to two peaks at 0.93 nm and 0.4 nm after crosslinking. The large peak at 0.93 nm was most likely a result of the intercalation of EDA into GO layers during the crosslinking process, while the small peak at 0.4 nm was possibly caused by the slight reduction of oxygen functional groups due to heating in the crosslinking process.

The hydrazine reduction after EDA crosslinking further increased the N content to 9.8%, and decreased the O content to 20.4% (Fig. 3A), obviously changing in the membrane structure. As shown in Fig. 3B, although the two peaks after hydrazine reduction (rcGO) are only shifted to locations associated with slightly smaller values (0.93 to 0.89 nm, and 0.4 to 0.35 nm), both peaks are

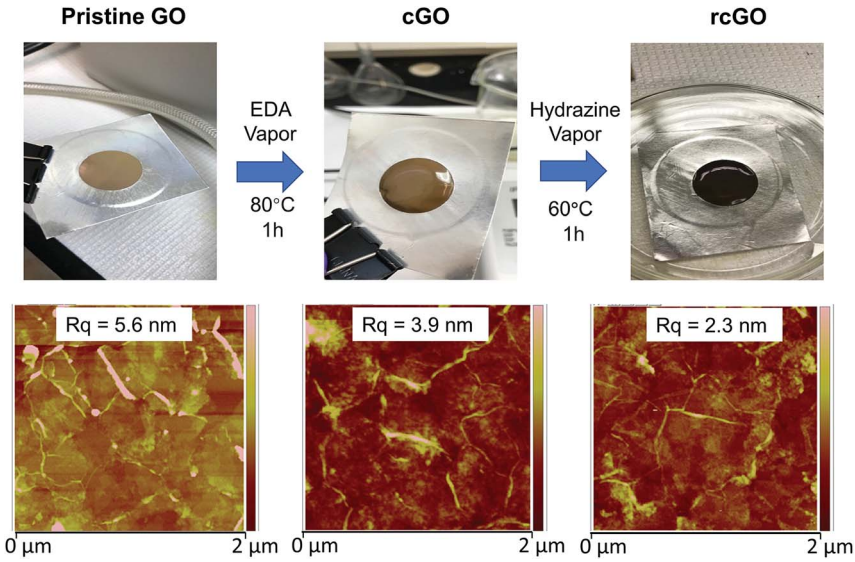

Fig. 2 Morphology of pristine, EDA-crosslinked, and hydrazine-reduced GO membranes.

significantly widened compared with those for cGO, indicating that the reduction process greatly broadened the distribution of membrane interlayer spacing. In addition, the peak for the 0.35 nm interlayer spacing becomes dominant after hydrazine reduction, suggesting that the oxygenated functional groups from carbon plane were removed, collapsing the wider nanochannels to narrow ones, which were similar in size to pristine graphene nanochannels.

Effectiveness of EDA crosslinking in controlling GO membrane swelling

GO membrane swelling is caused by the intercalation of water molecules into the interlayer spacing of the GO structure in an humid/aqueous environment. Crosslinking has been a common way to prevent the swelling and thus enhance the stability and separation performance of GO membranes. So far, most studies

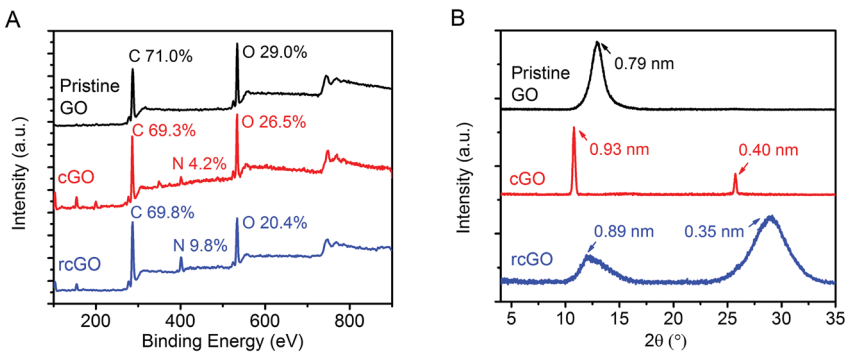

Fig. 3 Characterization of the elemental composition by XPS (A) and interlayer spacing by XRD (B) of the dry pristine GO, cGO and rcGO membranes.

have relied on rejection data to indirectly assess various crosslinking strategies for swelling control.[10,15] In this study, we used an integrated QCM-D/ellipsometry online monitoring system to directly measure the interlayer spacing of GO membranes before and after crosslinking in various humid environments to prove the effectiveness of crosslinking for swelling control. In addition, we chose EDA as crosslinker because the short chain (only a two-carbon chain) of small EDA molecules is expected to provide more rigid bonding between GO layers to prevent swelling.

As shown in Fig. 4A and B, the pristine GO membrane experienced significant swelling when exposed to a humid environment, and the increase in thickness and interlayer spacing is more obvious than the increase in mass. Specifically, the

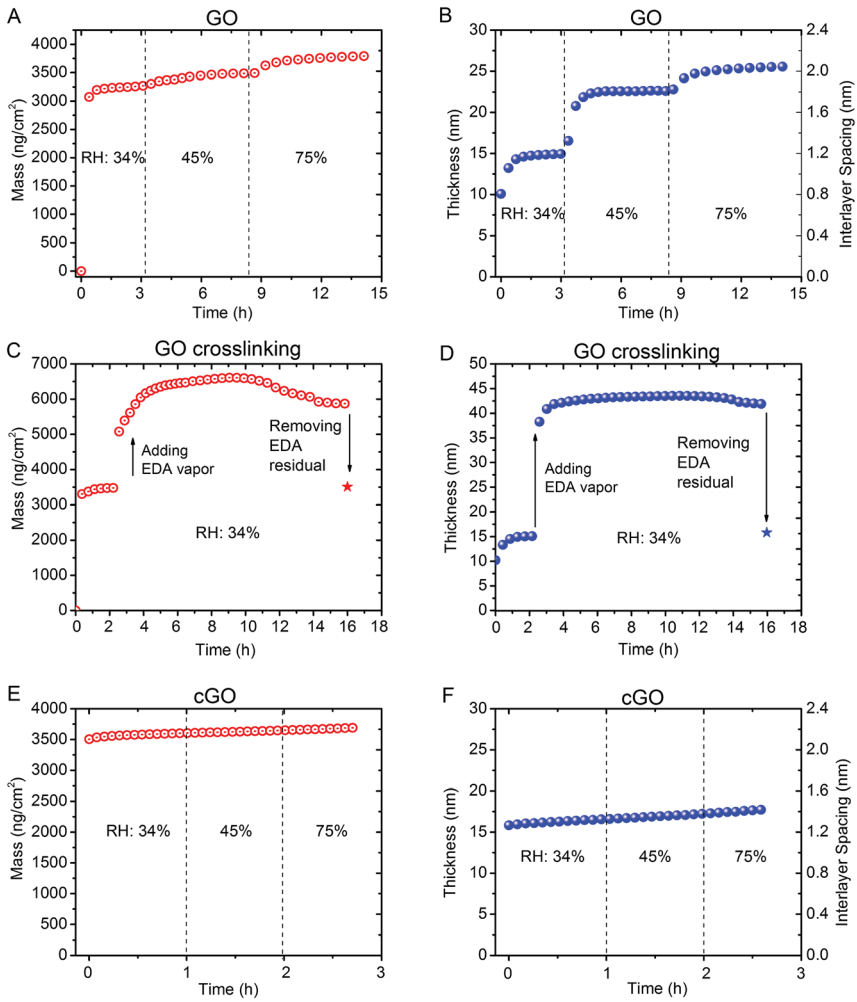

Fig. 4 The online monitoring of GO membrane swelling in terms of changes in membrane mass, thickness, and interlayer spacing: (A and B) pristine GO membrane under different relative humidity (RH) conditions, (C and D) GO membrane during the EDA crosslinking process at a RH of 34%, and (E and F) EDA-crosslinked (cGO) membrane under different RH conditions.

interlayer spacing of the pristine GO membrane increased from 0.79 nm under dry conditions (Fig. 3B) to 1.2, 1.8, and 2.1 nm in environments with relative humidities of 34%, 45% and 75%, respectively. To control swelling, EDA vapor was used to crosslink the GO membrane equilibrated at a relative humidity of 34% and resulted in an interlayer spacing of 1.2 nm. Fig. 4C and D show that, during the initial stage of crosslinking, both the mass and thickness of the membrane increased dramatically mainly due to the condensation and adsorption of EDA vapor on the membrane. After the crosslinking reaction, the resulting cGO membrane was thoroughly cleaned with DI water to remove unreacted EDA residue. The mass and thickness of the cleaned cGO membrane were only slightly larger than those of the pristine GO membrane.

Next, the swelling behavior of the cGO membrane was studied under different humidity conditions. As shown in Fig. 4E and F, both the mass and thickness of the cGO membrane almost remained constant as the relative humidity increased from 34% to 75%, and the interlayer spacing stayed in a narrow range of 1.3 to 1.4 nm, proving that EDA crosslinking is very effective in preventing the GO membrane from swelling. Note that the interlayer spacing of a cGO membrane in humid air is about 0.4 nm larger than the interlayer spacing of 0.93 nm in a completely dried cGO membrane (Fig. 3B). Therefore, water molecules can still intercalate into the 2D channels of a cGO membrane, but the EDA crosslinkers are able to hold the nanosheets in place to prevent the nanochannels from expansion.

Effects of GO crosslinking and reduction on water and ion transport

The knowledge about the effectiveness of crosslinking in preventing GO swelling and hence maintaining a relatively constant interlayer spacing enables a clear understanding of water and ion transport within the GO membrane. Using $MgCl_2$ and Na_2SO_4 as representative divalent salts, we tested the water flux and rejection of the PES membrane support as well as the pristine GO, cGO, and rcGO membranes. As shown in Fig. 5, the deposition of pristine GO onto the PES support decreased the water flux from ~22 to ~18 LMH bar^{-1} and the salt rejection was entirely contributed to by the deposited GO layers since the PES support alone contributed nothing. The pristine GO membrane exhibited very low $MgCl_2$ rejection (10%), which was likely attributed to membrane swelling in

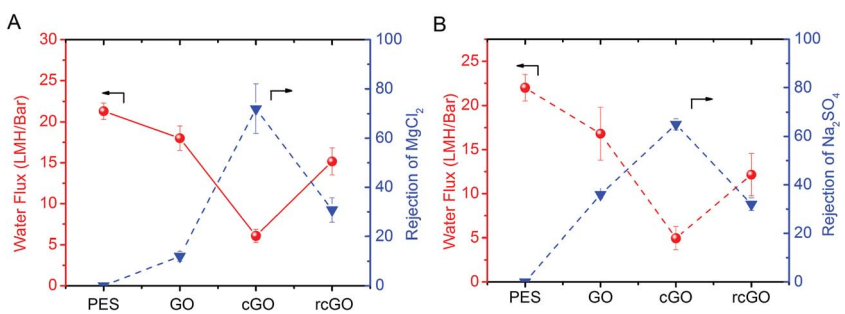

Fig. 5 The water flux and rejection of $MgCl_2$ (A) and Na_2SO_4 (B) by the PES support, pristine GO, cGO, and rcGO membranes, tested in an RO system under 14 bar and 100 mM of each ion in feed solution.

$MgCl_2$ solution with enlarged interlayer spacing reaching around 7 nm.[9] The slightly higher rejection (~40%) of Na_2SO_4 was consistent with our previous observation that GO membranes swell much less in Na_2SO_4 solutions, which results in an interlayer spacing of around 2 nm.[9] After crosslinking, the water flux of the cGO membrane decreased to around 5–6 LMH bar^{-1} and the rejection of both $MgCl_2$ and Na_2SO_4 increased to ~70%, which is consistent with the narrowed interlayer spacing of cGO (Fig. 4F) due to the prevention of membrane swelling.

The subsequent reduction of the cGO membrane caused the water flux to increase by almost 150% reaching 12–15 LMH bar^{-1}. Such a dramatic flux enhancement indicated that the partial removal of oxygenated functional groups by reduction likely decreased the resistance to water transport within the GO channels. To further understand the effect of GO reduction on water transport, we investigated the water flow within GO and graphene channels using MD simulation. Fig. 6A and B show the constructed MD model of GO nanosheets and the layered structure of GO membranes solvated into water, respectively. An interlayer spacing of 3 nm was used in the simulation to represent the swelled GO structure in an aqueous environment. As shown in Fig. 6C, the water transport velocity in a GO channel at each of the studied pressures (250, 500, and 1000 bar) is distributed parabolically, where the horizontal coordinate represents the location of the water layer along the channel height, with the origin defined at the center of the GO channel. Note that in order to obtain precise data for water flux within a finite simulation time the pressure used in the simulation was higher than that used in a real filtration process (typically less than 100 bar). As a comparison, the water transport velocity in a graphene channel was also simulated using the same nanosheet lateral dimension and interlayer spacing and under the same pressure (Fig. 6D). It is clearly seen that the velocity of water flow between pristine graphene sheets is almost two orders of magnitude higher than that in the GO

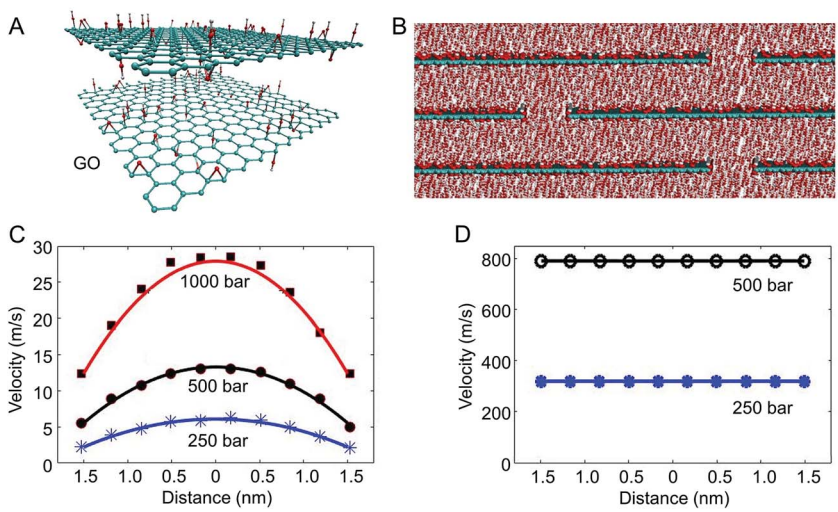

Fig. 6 The atomic structure of GO nanosheets (A), the layered GO structure solvated in water used in MD simulation (B), and the MD-simulated velocity profiles of water transport in a GO channel (C) and a graphene channel (D).

membrane, indicating that a remarkable boundary slip exists due to the diminishing friction at the liquid–solid interface by removing the extruding oxygenated functional groups from the carbon wall. The nearly horizontal velocity profile of the graphene channel in Fig. 6D demonstrated that the dramatic flux enhancement is attributed to the extreme slippage of water on the hydrophobic surface.

Note that the reduction of the cGO membrane also resulted in a decrease of salt rejection to about 30%, which is likely due to a weakened charge screening effect because of the removal of charged oxygenated functional groups. It is also interesting to note that the reduction somehow widened the distribution of interlayer spacing (Fig. 3B), which could contribute to the decrease in salt rejection as well.

Conclusions and implications

In this investigation, we proved that the crosslinking of layer-stacked GO membranes by small EDA molecules is an effective strategy to prevent membrane swelling in water and generate a relatively constant interlayer spacing of ~1.3 nm that enables the separation of divalent salts. However, although high water flux has been a major motivation of developing GO membranes for water-related applications, unlike the extreme slippage of water on the smooth graphene walls that results in very high water transport velocity, the presence of extruding functional groups on the GO plane dramatically slows down water transport in GO channels. In an effort to decrease the 2 orders of magnitude difference in water transport velocity between graphene and GO channels, the membrane reduction by hydrazine is effective in partially removing the functional groups on the GO plane and improving water flux by about 150%. However, the membrane reduction also results in a decrease in salt rejection due to a weakened charge screening effect and somehow widened interlayer spacing, indicating that it is necessary to further narrow the interlayer spacing to enable exclusive salt rejection by size exclusion.

In summary, these findings on GO structure and water transport provide a necessary basis for further tailoring and optimizing the design and fabrication of GO membranes in various separation applications. To simultaneously achieve high permeability and high salt rejection, it is critical to generate 2D nanochannels with precisely controlled interlayer spacing that does not swell in aqueous solutions and with smooth channel walls that do not interrupt water transport. It is promising to obtain such an ideal nanostructure by creating van der Waals heterogeneous layers with carefully selected and designed 2D nanomaterials.

Conflicts of interest

There are no conflicts to declare.

Acknowledgements

The material is based upon work supported by the U.S. National Science Foundation under award no. CBET-1565452 and CBET-1706059. The opinions expressed herein, however, are those of the authors and do not necessarily reflect those of the sponsors.

References

1 B. X. Mi, Graphene oxide membranes for ionic and molecular sieving, *Science*, 2014, **343**(6172), 740–742.
2 R. K. Joshi, P. Carbone, F. C. Wang, V. G. Kravets, Y. Su, I. V. Grigorieva, H. A. Wu, A. K. Geim and R. R. Nair, Precise and ultrafast molecular sieving through graphene oxide membranes, *Science*, 2014, **343**(6172), 752–754.
3 F. Guo, M. Creighton, Y. T. Chen, R. Hurt and I. Kulaots, Porous structures in stacked, crumpled and pillared graphene-based 3D materials, *Carbon*, 2014, **66**, 476–484.
4 Z. An, O. C. Compton, K. W. Putz, L. C. Brinson and S. T. Nguyen, Bio-inspired borate cross-linking in ultra-stiff graphene oxide thin films, *Adv. Mater.*, 2011, **23**(33), 3842–3846.
5 F. Perreault, A. Fonseca de Faria and M. Elimelech, Environmental applications of graphene-based nanomaterials, *Chem. Soc. Rev.*, 2015, **44**(16), 5861–5896.
6 R. K. Joshi, S. Alwarappan, M. Yoshimura, V. Sahajwalla and Y. Nishina, Graphene oxide: The new membrane material, *Applied Materials Today*, 2015, **1**(1), 1–12.
7 A. Nicolai, B. G. Sumpter and V. Meuniera, Tunable water desalination across graphene oxide framework membranes, *Phys. Chem. Chem. Phys.*, 2014, **16**(18), 8646–8654.
8 M. Hu and B. Mi, Enabling graphene oxide nanosheets as water separation membranes, *Environ. Sci. Technol.*, 2013, **47**(8), 3715–3723.
9 S. Zheng, Q. Tu, J. J. Urban, S. Li and B. Mi, Swelling of graphene oxide membranes in aqueous solution: Characterization of interlayer spacing and insight into water transport mechanisms, *ACS Nano*, 2017, **11**(6), 6440–6450.
10 A. Klechikov, J. Yu, D. Thomas, T. Sharifi and A. V. Talyzin, Structure of graphene oxide membranes in solvents and solutions, *Nanoscale*, 2015, **7**(37), 15374–15384.
11 L. Jin, Z. Wang, S. Zheng and B. Mi, Polyamide-crosslinked graphene oxide membrane for forward osmosis, *J. Membr. Sci.*, 2018, **545**, 11–18.
12 S. Zheng and B. Mi, Emerging investigators series: Silica-crosslinked graphene oxide membrane and its unique capability in removing neutral organic molecules from water, *Environ. Sci.: Water Res. Technol.*, 2016, **2**(4), 717–725.
13 Z. Jia, Y. Wang, W. Shi and J. Wang, Diamines cross-linked graphene oxide free-standing membranes for ion dialysis separation, *J. Membr. Sci.*, 2016, **520**, 139–144.
14 W. S. Hung, C. H. Tsou, M. De Guzman, Q. F. An, Y. L. Liu, Y. M. Zhang, C. C. Hu, K. R. Lee and J. Y. Lai, Cross-linking with diamine monomers to prepare composite graphene oxide-framework membranes with varying *d*-spacing, *Chem. Mater.*, 2014, **26**(9), 2983–2990.
15 R. R. Nair, H. A. Wu, P. N. Jayaram, I. V. Grigorieva and A. K. Geim, Unimpeded permeation of water through helium-leak-tight graphene-based membranes, *Science*, 2012, **335**(6067), 442–444.
16 M. Hu and B. Mi, Layer-by-layer assembly of graphene oxide membranes *via* electrostatic interaction, *J. Membr. Sci.*, 2014, **469**, 80–87.

17 Y. Oh, D. L. Armstrong, C. Finnerty, S. Zheng, M. Hu, A. Torrents and B. Mi, Understanding the pH-responsive behavior of graphene oxide membrane in removing ions and organic micropollutants, *J. Membr. Sci.*, 2017, **541**, 235–243.
18 D. Van Der Spoel, E. Lindahl, B. Hess, G. Groenhof, A. E. Mark and H. J. Berendsen, Gromacs: Fast, flexible, and free, *J. Comput. Chem.*, 2005, **26**(16), 1701–1718.
19 W. Humphrey, A. Dalke and K. Schulten, Vmd: Visual molecular dynamics, *J. Mol. Graphics*, 1996, **14**(1), 33–38.
20 W. L. Jorgensen and J. Tirado-Rives, The opls [optimized potentials for liquid simulations] potential functions for proteins, energy minimizations for crystals of cyclic peptides and crambin, *J. Am. Chem. Soc.*, 1988, **110**(6), 1657–1666.
21 N. R. Tummala and A. Striolo, Role of counterion condensation in the self-assembly of SDS surfactants at the water–graphite interface, *J. Phys. Chem. B*, 2008, **112**(7), 1987–2000.
22 N. Patra, B. Wang and P. Král, Nanodroplet activated and guided folding of graphene nanostructures, *Nano Lett.*, 2009, **9**(11), 3766–3771.
23 H. Berendsen, J. Grigera and T. Straatsma, The missing term in effective pair potentials, *J. Phys. Chem.*, 1987, **91**(24), 6269–6271.
24 Z. Wang, Q. Tu, S. Zheng, J. J. Urban, S. Li and B. Mi, Understanding the aqueous stability and filtration capability of MoS_2 membranes, *Nano Lett.*, 2017, **17**(12), 7289–7298.
25 S. Nosé, A unified formulation of the constant temperature molecular dynamics methods, *J. Chem. Phys.*, 1984, **81**(1), 511–519.
26 W. G. Hoover and C. Hoover, Nonequilibrium molecular dynamics, *Condens. Matter Phys.*, 2005, **8**(2), 42.
27 U. Essmann, L. Perera, M. L. Berkowitz, T. Darden, H. Lee and L. G. Pedersen, A smooth particle mesh Ewald method, *J. Chem. Phys.*, 1995, **103**(19), 8577–8593.
28 E. A. Cino, J. Wong-Ekkabut, M. Karttunen and W.-Y. Choy, Microsecond molecular dynamics simulations of intrinsically disordered proteins involved in the oxidative stress response, *PLoS One*, 2011, **6**(11), e27371.

